QUASI-STEADY SOLAR WIND DYNAMICS

V. J. Pizzo
High Altitude Observatory
National Center for Atmospheric Research[*]
P. O. Box 3000
Boulder, CO 80307 USA

ABSTRACT

This paper opens with a brief review of recent progress in understanding the large scale dynamics of quasi-steady, corotating solar wind structure. It then focuses on two new study areas that these observational and theoretical advances have made ripe for development. The first concerns the nature of the solar wind at large heliocentric distances ($r > 10$AU). Preliminary calculations from a 2-D MHD model are used to demonstrate theoretical expectations of corotating structure out to 30 AU. It is found that the forward and reverse shocks from adjacent CIR's begin to interact at about 10 AU, producing new shock pairs flanking "secondary" CIR's. These sawtooth secondary CIR's interact again at about 20 AU and survive as visible entities (though not necessarily as shocks) to 30 AU. The model predicts the velocity jumps at the leading edge of the secondary CIR's at 30 AU should be very small but there should still be sizable variations (factor of 2-3 jumps at the CIR fronts) in the thermodynamic and magnetic parameters, with considerable remnant substructure to be seen. The most important points are that the driving dynamic mechanism in the distant solar wind is the relaxation of pressure gradients (not kinematic steepening, as in the near-sun solar wind) and that the models make a number of definite, quantitative predictions that can be compared with available data. The second topic is the influence of weak, non-impulsive time dependence in quasi-steady dynamics. It is suggested that modest (~ 75km/s) large scale variations in the coronal flow speed on periods of several hours to a day (presumably associated with the continual coronal evolution) may be responsible for many of the remaining discrepancies between theory and observation. In particular, such temporal effects offer a ready explanation for the apparent rounding (or de-steepening) of stream fronts between 0.3 and 1.0 AU discovered by Helios.

Introduction

The last several years have witnessed a steady enrichment of our understanding of corotating stream dynamics. On the empirical front, Helios has returned marvelous data on the near-sun solar wind, while Pioneer and Voyager probe ever deeper into the far reaches of the heliosphere. Coupled with observations from numerous other spacecraft at intermediate distances, the quantity and quality of relevant data available to researchers today is truly impressive. On the theoretical front, description of interplanetary dynamics has achieved a high level of sophistication, such that most of the physical mechanisms thought to be important in the large scale evolution of corotating structures are now included in the models.

My main theme is that the conjunction of all this observational and theoretical progress finally makes it feasible to tackle certain long-standing problems with a reasonable chance of success. In this discussion, I will single out two topics I find particularly

---

enticing and potentially rewarding, though these by no means exhaust the possibilities. Specifically, the questions I will concentrate on are: 1) What is the nature of the distant $(r>10$ AU) solar wind and does it differ very much from the familiar near-sun $(0.3<r<5AU)$ flow? 2) To what extent do slow, non-impulsive temporal variations in the coronal source regions of the solar wind affect the interplanetary evolution of steam structures, i.e.; What happens when the flows are really only quasi-steady as opposed to absolutely steady as idealized in the models?

Background for the Discussion

We begin with a brief review, largely theoretical, of the current state-of-the-art in the field of corotating stream dynamics. A schematic representation of the classic interplanetary stream interaction phenomenon is depicted in Figure 1, in which we view the flow in the solar equatorial plane from over the north pole of the sun. Alternating regions of nearly radial fast and slow flow originating in the corona are indicated by long and short dark arrows. Under the influence of solar rotation, fast flows near the sun are brought into radial alignment with more distant slow flows emitted earlier; as the former overtake the latter, the intervening material is compressed and heated (shaded area), which in turn drives small but dynamically important nonradial flows (large open arrows). If this compression is vigorous enough, a forward and reverse corotating shock pair may result further out. In regions where fast material outraces succeeding slow plasma, a relative rarefaction is formed. The magnetic field (light lines) is drawn out into a spiral configuration, whose pitch depends upon the flow speed. As the entire pattern rotates with the sun, a spacecraft situated at, say, 1 AU will see an apparent temporal variation, with most of the interesting dynamics confined to the leading edge of the high-speed stream.

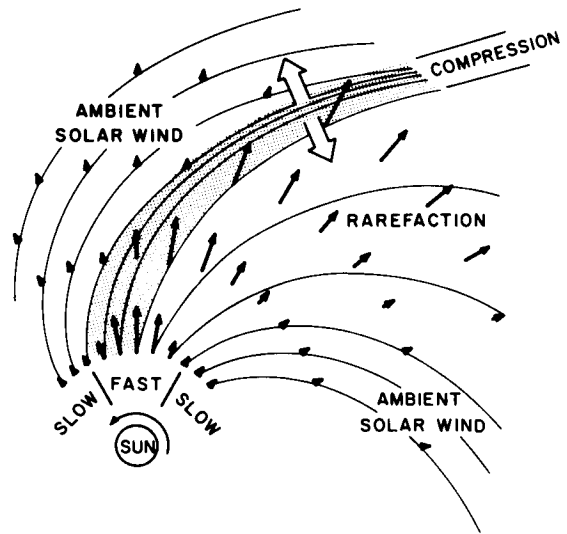**STREAM INTERACTION SCHEMATIC
(INERTIAL FRAME)**

Figure 1). Stream-interaction schematic in the solar equatorial plane.

Quantitative theoretical description of these interactions has been most successfully formulated in terms of continuum MHD. For steady, superalfvenic flow in interplanetary space, the appropriate equations in a frame corotating with the sun are (in cgs units):

$$\nabla \cdot \rho \vec{v} = 0 \tag{1}$$

$$\rho[(\vec{v} \cdot \nabla)\vec{v} + 2\vec{\Omega} \times \vec{v} + \vec{\Omega} \times (\vec{\Omega} \times \vec{r})] = -\nabla P - \rho \frac{GM_s}{r^2} \hat{r} + \frac{(\nabla \times \vec{B}) \times \vec{B}}{4\pi} \tag{2}$$

676

$$\nabla \cdot \left[\vec{v} \left(\rho \frac{\vec{v} \cdot \vec{v} - |\vec{\Omega} \times \vec{r}|^2}{2} + \frac{\gamma}{\gamma - 1} P \right) + \frac{\vec{B} \times}{4\pi} (\vec{v} \times \vec{B}) \right] = -\rho \frac{GM_s v_r}{r^2} \hat{r} \qquad (3)$$

$$\nabla \cdot \vec{B} = 0 \qquad (4)$$

The dependent variables are: mass density, $\rho = mn$, where m is the proton mass and n the proton number density; velocity, $\vec{v}$; isotropic gas pressure, P; and magnetic field, $\vec{B}$. The other symbols are: the solar equatorial rotation rate, $\vec{\Omega}$; the spherical radius vector, $\hat{r}$; the universal gravitational constant, G; the solar mass, M_s; and the polytropic index, γ.

Among the important assumptions entering into the derivation of these equations are that the plasma behaves like an electrically neutral proton-electron fluid, that the electrical conductivity is infinite, and that the electric field in the rotating frame is zero. Heat conduction, viscosity (except at shocks), wave dissipation, and all kinetic-level effects are taken as having negligible impact upon the large scale dynamics. Hence the gas pressure is isotropic and related to the proton and electron temperatures T_p and T_e by the auxiliary relation

$$P = nk(T_p + T_e) = 2nkT \qquad (5)$$

where k is Boltzmann's constant and T is the single-fluid temperature. The internal energy is governed by a polytrope law, so that

$$(\vec{v} \cdot \nabla) P \rho^{-\gamma} = 0. \qquad (6)$$

All these approximations are reasonably justifiable in the momentum-dominated superalfvenic solar wind at, say, 0.3 AU and beyond. It should be borne in mind, however, that many of the above assumptions may prove untenable closer to the sun and almost certainly break down in the corona, which is, by clever design, outside the scope of this paper.

Even with all these restrictions, quite a variety of models can be constructed from equations 1-6. The differences among them are best discussed within the context of 2-D (planar) flows in the solar equatorial plane (three dimensional aspects of the problem will be addressed below.) By virtue of the assumptions introduced previously, all the interesting physical content of the formulation resides in the momentum equation (2). This circumstance provides a convenient means of classifying the models. The most fundamental distinction one can draw is between kinematic and dynamic formulations. The terms on the left-hand-side of (2) constitute the purely kinematic portion of the description: the velocity gradients couple with solar rotation to regulate the rate at which material is compressed or rarefied. The terms on the right-hand-side of (2) embody the truly dynamic part of the interaction: gas pressure and field gradients determine what happens once the kinematic action brings fluid elements together. (Gravitational effects are negligible in interplanetary space and are carried along for completeness only because it is a numerically trivial operation.) Purely kinematic models ($P = \vec{B} = 0$) are attractive in that they are nonlinear while retaining extreme computational simplicity (e.g. see Matsuda and Sakurai, 1972; Burlaga and Barouch, 1976.) The problem with that approach, however, is that for the kinds of structures most commonly encountered in the near-sun solar wind (i.e., sharply-bounded high-speed streams), the dynamical reaction of the gas has a profound effect upon the rate of steepening and shock formation and the resultant structure of the interaction front. Furthermore, in the distant solar wind ($>10 AU$), where the initial high-speed material contained in the streams has been completely expended,

the subsequent interactions are driven entirely by secondary pressure waves. That is, there is hardly any kinematics left in the problem (see next section). Thus, while use of kinematic models for limited illustrative purposes, for crude tracing of the solar origin of broad interplanetary streams (e.g. Nolte et al., 1977), and for judicious mapping of select portions of streams well away from interaction regions may be warranted, on the whole they are quantitatively and sometimes even qualitatively inadequate. (For further discussion on this point, see Pizzo, "Comments on the Paper by Akasofu and Hakamada", this Conference.)

Among the dynamic models, the computationally simplest formulation is the linear model originally developed by Carovillano and Siscoe (1969). Unfortunately, this model, too, suffers a very severe flaw in that the amplitude of the variations in the solar wind are so large as to preclude a linear evolution over any but the shortest distances and the most favorable conditions (no large velocity gradients). Hence it is generally unacceptable for typical solar wind applications. The model of Hundhausen (1973a) overcomes these objections through the incorporation of both nonlinear steepening and gas pressure forces. Despite its merits, this model, too, harbors certain deficiencies that restrict its utility. Namely, it neglects the magnetic forces and the secondary nonradial flows built up in the interaction. These nonradial flows, while small, are now known to significantly relieve the compressive stresses generated at the stream front by allowing lateral slippage of the fluid, thereby retarding both the steepening and shock formation. The magnetic field has a similar, though two-fold, effect: first, the fluid has greater resistance to direct compression by virtue of the magnetic pressure gradients; and, second, the relevant characteristic speed in the fluid becomes the fast-mode speed (which is normally about twice the sound speed in interplanetary space), which means the pressure forces can more effectively distribute the compressive stresses over a larger volume of the fluid. Neglect of the nonradial flow is not too bad so long as only streams with broad boundaries are considered or attention is restricted to flows beyond 1 AU (Gosling et al., 1976; Dryer et al., 1978). However, as demonstrated by Helios (Rosenbauer, et al. 1977), streams near 0.3 AU in fact tend to have sharp boundaries. Models of the Hundhausen (1973a) type, even with some allowance for field effects (Steinolfson et al., 1975), perform poorly under such conditions, seriously overestimating the rate of steepening and shock formation.

Proper description of corotating stream dynamics is thus seen to demand at least the full formalism contained in equations (1) - (4): nonlinearity, nonradial flows, and magnetic and gas pressure effects. Models incorporating all these properties (Goldstein, 1971; Goldstein and Jokipii, 1977; Whang and Chien, 1981; Pizzo, 1982) are capable of reproducing to a reasonable approximation the sort of large scale phenomena typically observed by spacecraft over a broad range of heliocentric distances. Figures 2 and 3 illustrate an example from one such model (Pizzo, 1982). The curves in Figure 2 depict the variation of radial velocity, density, and temperature across the stream on an initial surface taken to lie at 0.3 AU, well outside the critical points. The nonradial velocity is set to zero there, while the field magnitude is held constant across the structure at a uniform value, $|\vec{B}| = 45\gamma$. This input is an idealization of the 1975 Helios perihelion observations, in which dense, slow, cold flow alternated with hot, tenuous, fast flows in a step-function-like manner. When this structure is propagated to 1 AU via a suitable numerical integration of equations (1) -(6), the longitudinal variations recorded in Figure 3 result. As fast material overtakes slow at the stream front, the compressive interaction gives rise to forward (F) and reverse (R) large-amplitude MHD waves which propagate in opposite directions away from the interaction front. (In this example they have steepened into shocks, though for other choices of intial conditions they need not. See also Whang and Chien, 1981). Sandwiched in between is a shear-flow interface (I), which arises as a natural consequence of the radial compression along the spiral front (Hundhausen and

Burlaga, 1975; Gosling *et al.*, 1978). The density, temperature, and field strength all vary in a fashion representative of 1 AU stream fronts (Siscoe, 1972; Gosling *et al.*, 1972).
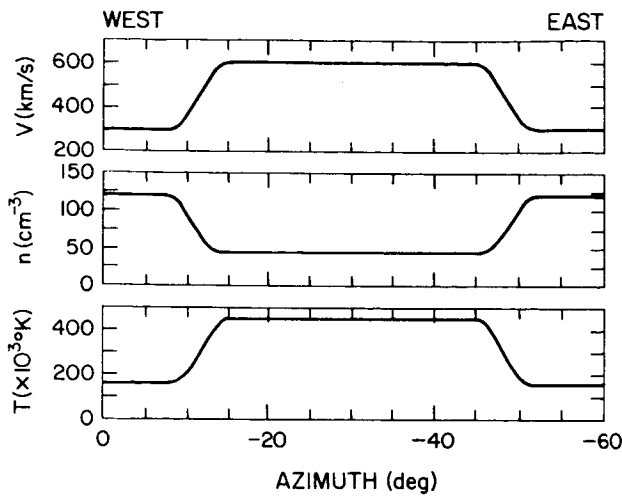

Figure 2). Input variations for hypothetical stream at 0.3 AU. Also, on this initial surface, the flow angle $\phi = 0$ and $|\vec{B}| = 45\gamma$. These parameters are chosen to mimic Helios perihelion data (Rosenbauer et al. 1977). Periodic boundary conditions are imposed at the two longitudinal ends.
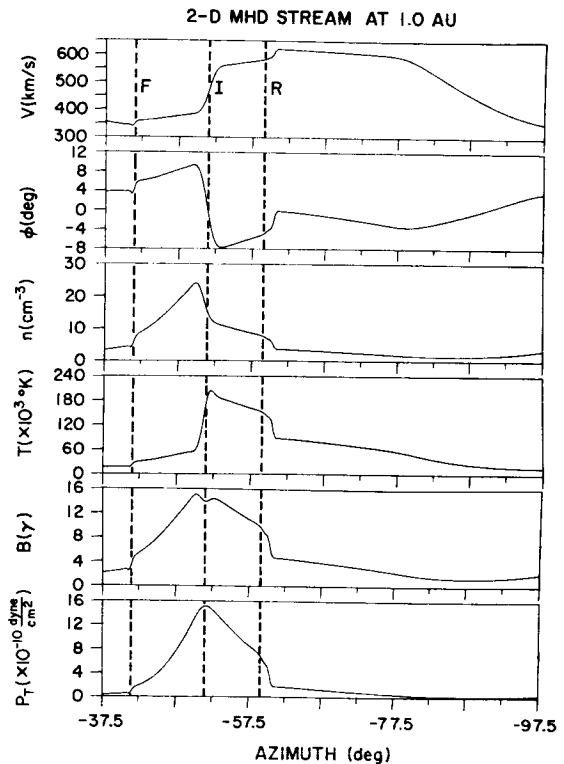

Figure 3). Appearance of the stream in Figure 2 at 1.0 AU, according to a 2-D MHD model (Pizzo, 1982). F and R refer to forward and reverse shocks, while I denotes the shear-flow interface that evolves between the high-speed and low-speed regimes. P_T is the total (gas plus magnetic) pressure.

Of course, the 3-D structure of the corona must somehow be impressed upon the solar wind, so it is natural to ask whether global effects might not seriously alter the evolution from the 2-D idealization. Owing to the limited and fragmented 3-D data currently available, the only insight to be gained comes from 3-D MHD models using hypothetical, but hopefully relevant, input structures (Pizzo, 1982; see also Riesebieter, 1977; Whang, 1980). The basic idea is to compare streams that have identical longitudinal variations at the equator but differ markedly in their geometry away from the equator. Figure 4 shows two 3-D geometries analyzed in the Pizzo (1982) study, here portrayed as contour plots of radial velocity on the r = 0.3 AU initial surface. On the left, we see a circular-shaped, sharply bounded stream centered at the equator. The radial velocity is 600 km/s throughout the middle of the stream, falling smoothly to 300 km/s all about its periphery. Temperature and density have the same correlation with velocity as in Figure 2, while both components of the nonradial flow are zero and $|\vec{B}| = 45\gamma$ as before. On the right, we find a geometry suggestive of a polar high-speed stream, where the velocity is 600 km/s except in a narrow 300 km/s band crossing the equator. Figure 5 compares the 1 AU solutions at the equator for 2-D (dashed), 3-D circular (solid), and 3-D polar (dotted) streams. As might be expected, the differences between the 2-D and 3-D circular projections are minimal. What is more intriguing is that the 3-D polar solution deviates so little from the other two, despite the discordant geometries. From this it can be inferred that
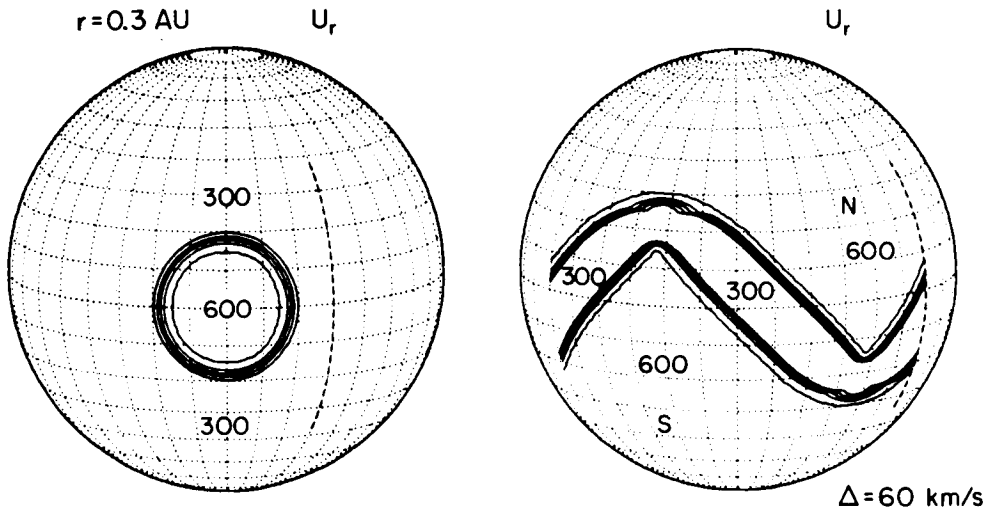
Figure 4). Constant velocity contours for two different 3-D geometries at the 0.3 AU spherical initial surface. The increment between contour levels is 60 km/s.

north-south flow effects generated by meridional gradients in the interplanetary 3-D solar wind are not too severe and that it should therefore be legitimate to use 2-D models for the mapping of flows. Nevertheless, this optimistic assessment must be tempered with the caution that it really applies only in the case that the global structure at the input be fairly regular, i.e., that the stream fronts especially contain no great amount of substructure (Pizzo, 1982). It is thus in the absence of any compelling evidence that such substructure is common that we tentatively justify the continued use of 2-D models.

Much more complete and detailed comparisons of these various models may be found in Pizzo (1978, 1981, 1982) and Steinolfson et al. (1975).
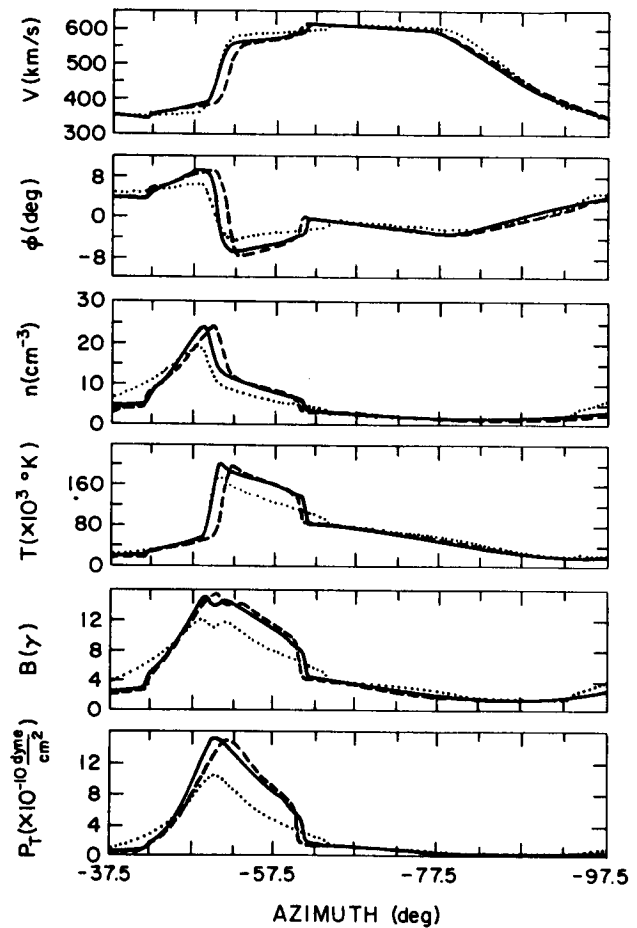

Figure 5). Comparison of 1 AU equatorial solutions of three models, showing effects of differing stream geometries: 2-D (dashed); 3-D circular (solid); and 3-D polar (dotted).

2-D Evolution of Corotating Structure
To Large Heliocentric Distances

The general picture of stream evolution outlined above can be said to be fairly well established in the inner solar system ($r < 5AU$). At least, this is the region in which numerical simulations based on MHD theory have been favorably compared with various sets of radially-aligned spacecraft data (e.g. Gosling *et al.*, 1976; Dryer *et al.*, 1978). This is not to say that important discrepancies between theory and observation do not exist or that the models are faithful in every detail (see last section, below); rather, only that the basic concept is sufficiently valid to permit us to speculate (as I will in the remainder of this talk) on new phenomena with some degree of confidence.

About a decade ago, there arose two conflicting viewpoints as to the nature of solar wind structure at large heliocentric distances. One school of thought (Jokipii and Davis, 1969) held that turbulent dissipation would efficiently smooth out both corotating and transient flows within a few AU of the sun, resulting in an essentially featureless solar wind expansion at large distances. The other view (Hundhausen, 1973b) suggested, on the basis of hydrodynamic considerations, that identifiable streams would survive far out into the solar system (tens of AU) and would be manifest there as sawtooth velocity structures, with either a shock or very steep gradients at the leading edge. Eventually, in the mid-70's Pioneer data settled the argument in favor of the latter alternative, at least out to 5 AU (Hundhausen and Gosling, 1976; Smith and Wolfe, 1976). Nevertheless, it should not be assumed that the entire story has been told, that the very distant solar wind ($\gtrsim 10$ AU) offers nothing really new. Quite the contrary, I intend to persuade you that the structure of the far solar wind should harbor exciting new phenomena and that even within the context of dynamical evolution of the sort invoked by Hundhausen (1973), the flow beyond 10 AU differs in fundamental ways from the near-sun expansion. My presentation draws heavily upon some preliminary calculations I have just completed, but the views to be expressed closely parallel those recently espoused by Burlaga (1983), which are based largely upon Voyager observations.

In my calculation, real solar wind flows in the ecliptic are projected from 1 AU to 30 AU under the assumption of ideal corotation. The input data for this study are hourly averages of IMP 7 and 8 plasma parameters from the MIT experiment and the associated magnetic field measurements from the GSFC magnetometer, all covering one solar rotation from a period late in 1977. The solar wind structure at that time was not as steady as one would like for a detailed mapping survey; but for the didactic purposes at hand they will serve quite adequately. The model used for the simulation is virtually identical to that described in Goldstein and Jokipii (1977), with only minor differences in numerical techniques. This is a slight variant of the standard 2-D MHD quasi-steady formalism laid out above, in that electron and proton pressures are accounted for separately, with the electron pressure following a polytropic expression like (6). (The electron polytropic index is $\gamma_e = 1.175$, in consideration of Sittler and Scudder, 1980.) The proton pressure and temperature at each step are derived from total energy conservation (3), thus arbitrarily channeling all the shock heating provided by the artificial viscosity into the protons. This dipolytropic treatment results in a somewhat more realistic description of the electron thermodynamics, but our findings do not depend very critically upon this detail. (A more complete explanation of the model and analysis of the flow structures of late 1977 will appear shortly in papers by Burlaga *et al.* and Pizzo *et al.*, in preparation.)

Figures 6a and 6b show a stacked sequence of speed and total pressure (gas plus magnetic) variations over the radial range 1-30 AU. The curves in each panel portray speed or total pressure as a function of an arbitrary longitude scale, which is shifted in the calculation to make the center of each panel track the average interplanetary spiral.

The increment between the panels is 2 AU (except for the top pair), so the radial evolution can be followed by reading down each plot. Any feature which moves faster or slower than the mean speed (averaged over the rotation) will appear to drift in longitude. For example, the shock fronts associated with the classic CIR's forming just beyond 2 AU expand laterally in the plots though, of course, their propagation is primarily radial. Finally, the speed scale reads 200-700 km/s (linear) for each plot, but the total pressure scale (logarithmic) changes in absolute value. However, the spread in any one pressure plot is always a factor of 1000:1, so shock strengths can always be directly gauged.
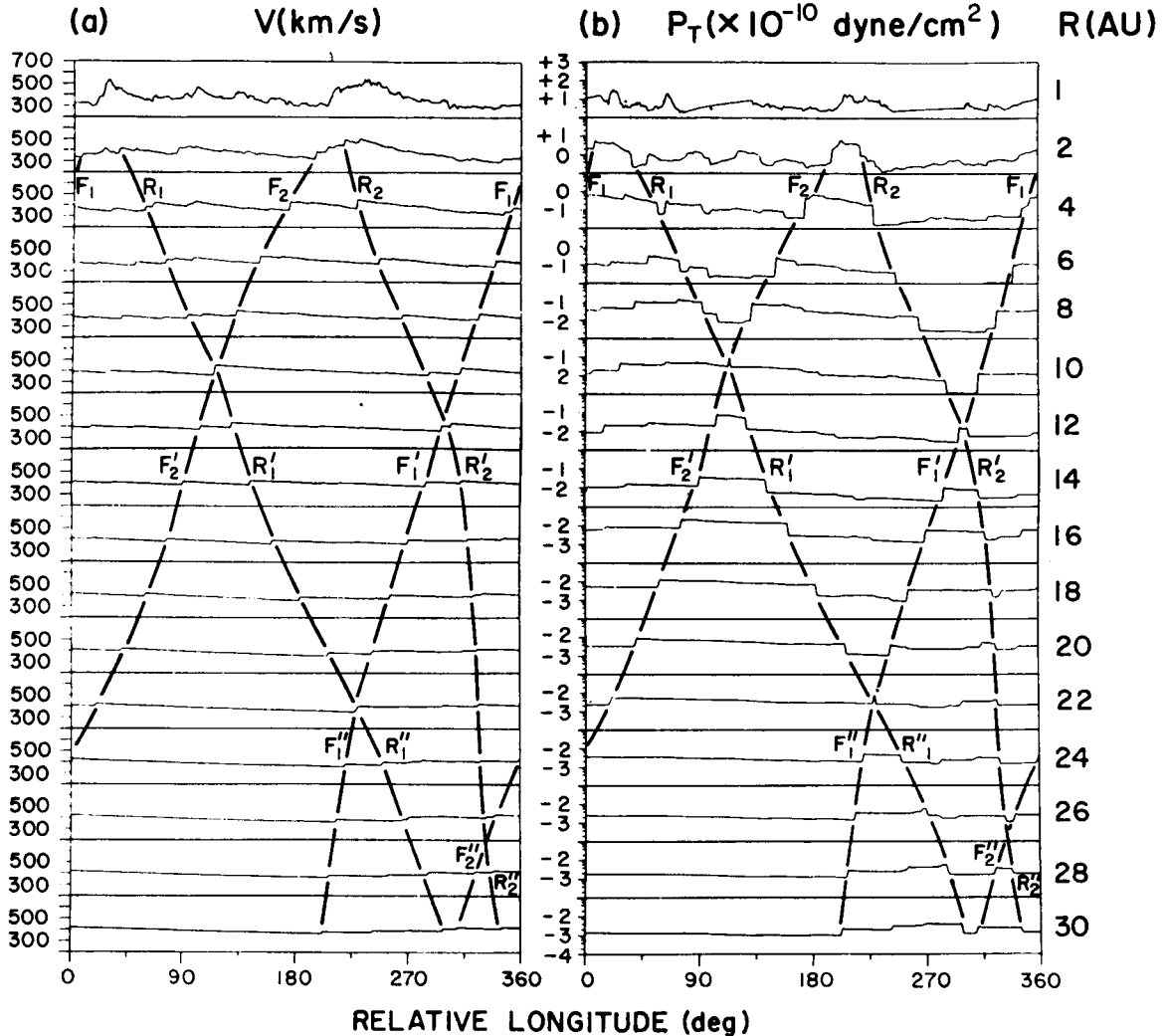

Figure 6). Bulk speed (a) and total pressure (gas + magnetic) (b) versus relative longitude for a solar rotation in late 1977. Heliocentric distance increases downwards. Data gaps in the 1 AU input have been filled in by linear interpolation and periodic boundary conditions are imposed at the longitudinal ends. The diagonal dark lines connect the main forward (F) and reverse (R) shock features, which propagate relative to the flow. Note the velocity scale is fixed; the pressure scale is variable, but always maintains a ratio of 1000:1 between maximum and minimum values. The digits just to the left of the pressure plots indicate the power of 10 by which the base value of 10^{-10} dyne/cm^2 must be multiplied to fix P_T, e.g. "+2" in the topmost panel denotes $P_T = 10^{-8}$ dyne/cm^2.

Examining the two figures, we see that out to 10 AU the evolution follows the classic steepening and CIR formation scenario well-known since Pioneer days. Forward and reverse shocks (heavy lines labelled F and R in the plots) form near 2 AU as the streams attain peak compression. The material trapped between finds itself at high pressure relative to its surroundings and begins pushing outwards from the center of the compressed region. Meanwhile, the material in the trailing portions is being steadily rarefied and cooled more rapidly than would a spherically-symmetric flow. Thus the shock strength, as measured by the pressure jumps in Figure 6b, increases rapidly between 2 and 4 AU and remains high out to 10 AU.

At 10 AU, near 120° longitude, something very interesting happens: the reverse shock (R_1) of the leftmost stream at 1 AU meets the forward shock (F_2) of the rightmost original stream. The ensuing interaction gives rise to a new, "secondary" CIR, which is characterized by elevated densities, temperatures, field strengths, and pressures and is flanked by the two modified incident shocks $(F_2'$ and $R_2')$, which have lost considerable strength (as judged by the jumps in total pressure) in the interaction. The other primary pair of shocks $(F_1$ and $R_2)$ meet with similar consequences at 12 AU, near 300° longitude. Both secondary CIR's subsequently expand, with additional interactions (accompanied by further CIR production and reduction in shock strength) at 22 AU, 26 AU, and again just beyond 30 AU. The interactions at 22 and 26 AU are of particular significance, in that shocks from successive Carrington rotations have had time to propagate all the way across the intervening structures and meet. Thus, by the latter point, the entire flow has been shocked at least once.

There are really three main points to be made here. The first is that the quasi-steady dynamics of the solar wind is driven by two distinct mechanisms. The near-sun evolution, out to 4-5 AU or so, is dominated by the familiar kinematic steepening mechanism. In this regime, the structure is characterized by the usual rotationally-coupled interaction of several discrete high-speed and low-speed flows. At about 5-10 AU, however, most of the speed differences have been eliminated and the evolution is instead regulated by the relaxation of pressure waves or pulses (i.e., the CIR's) generated by the previous kinematic interactions. By 8-10 AU, these pressure pulses are themselves beginning to interact, fostering further pressure pulse structure which survives to at least 30 AU. Hence the distant solar wind, even in the quasi-steady limit, differs qualitatively from the near-sun wind in that the primary interaction mechanism is dynamic rather than kinematic. Indeed, the very concept of streams *per se* is relevant only to the near-sun solar wind and has little bearing upon the dynamics of the distant solar wind (Burlaga, 1983).

To quantify these arguments, we turn to Figure 7, which presents a more detailed view of the 30 AU structure. From top to bottom, we have bulk speed, flow angle, density, field strength, proton temperature, and total pressure, respectively. Consider the shock jump near 200° longitude. It is most illuminating to think of the interaction between the faster flow to the right of the jump with the slower flow to the left in terms of a simple collision between two discrete blobs of gas. To an observer moving with the slower flow, the fast material (of density $n = 0.017 \text{cm}^{-3}$) is approaching with a velocity of $w \cong 15$ km/s (assuming a purely radial interaction); thus the fast material exerts a ram pressure of $\rho w^2 \cong 6.4 \times 10^{-14}$ dyne/cm^2. On the other hand, the total pressure differential across the jump is $\Delta P_T \cong 1.0 \times 10^{-13}$ dyne/cm^2. Since what matters are the relative momentum densities, it is evident that pressure forces are going to dominate in this distant solar wind interaction. This result stands in sharp contrast with the near-sun situation, which is readily illustrated by repeating the analysis on the 0.3 AU stream of Figure 2. Transforming to a frame moving with the 300 km/s slow flow, the high speed portion of the stream is found to possess a ram pressure of about 7.5×10^{-8} dyne/cm^2. For the example of Figure

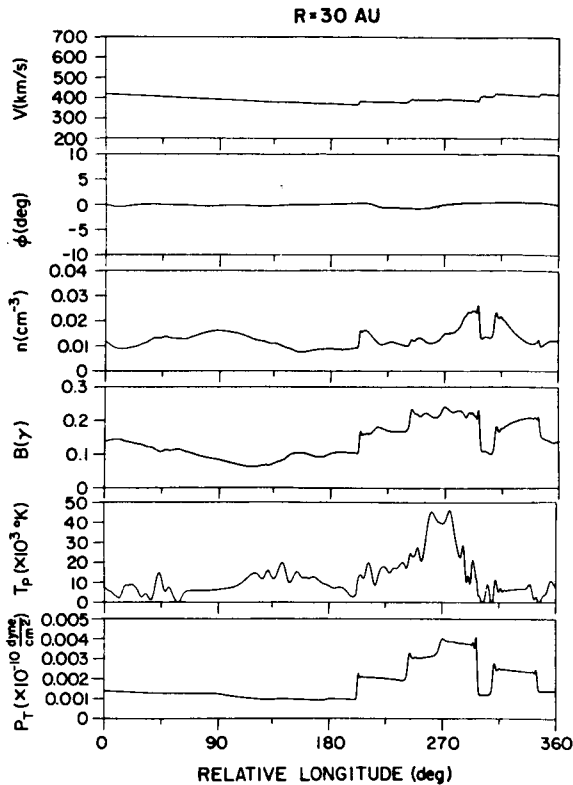**R = 30 AU**

Figure 7). Flow parameters at 30 AU for the streams of Figure 6.
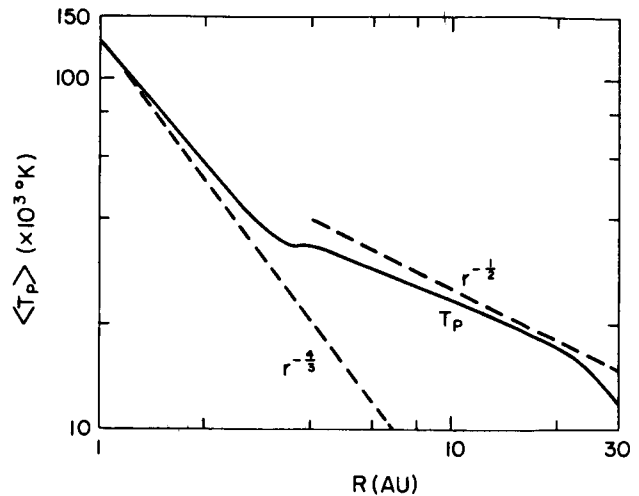

Figure 8). Longitudinally-averaged proton temperature for the streams of Figure 6. The two dashed lines provide theoretical adiabatic and tentative observed dependencies. In this model, the electrons follow a separate polytropic law ($\gamma_e = 1.175$) and the electron temperature goes approximately as $r^{-0.4}$.

2, ΔP_T was specifically chosen to be zero; but even were P_T in the stream doubled relative to that in the slow flow, ΔP_T would still amount to only 1.4×10^{-8} dyne/cm^2. Hence the mechanical advection clearly dominates near the sun.

A second major point is that the relatively dull 30 AU velocity structure portrayed in Figures 6a and 7 does not signify featureless flow, since streams can no longer be taken as the measure of inhomogeneity at these distances. While the variations in the flow speed at 30 AU are so small that the saw-tooth waveform might be very hard to discern in daily sample data of the type collected by Pioneer, the other four parameters show very sizable fluctuations, with pronounced (factor of 2-3) jumps across the CIR fronts. Note also that while the total pressure shows little variation between the big jumps, the density, field strength, and proton temperature all exhibit considerable substructure. This comes about because imbalances in total pressure directly give rise to forces that rapidly wipe out the total pressure gradient, whereas variations in the density, field strength, and temperature need not be individually obliterated to satisfy this condition. Furthermore, much of the magnetic and thermodynamic substructure evident in Fig. 7 is dynamically created in the medium. (the term "substructure" here applies only to numerically resolved features, such as the density and temperature enhancement accompanying the shock near 200° longitude. The higher-frequency oscillations right at the shocks are spurious numerical artifacts.) Refering once more to Figure 6, a number of other propagating features in addition to the two main shock pairs can be traced, smaller amplitude forward and reverse structures (not necessarily shocks) that exist only over a limited span of heliocentric distances. Some of these originate from the real input

structure, some are artifacts of the linear interpolation used to fill data gaps, and some are generated further out by the interaction of the larger CIR fronts with the ambient structure. The resultant thermodynamic structure at 30 AU thus bears virtually no resemblance to the parent 1 AU variations.

Just how realistic these calculations and, indeed, this entire picture of the distant solar wind are remains to be seen. After all, even if the model itself proves substantially accurate, we have here mapped only the flows associated with the streams of one particular rotation. The larger streams associated with the Skylab epoch, for example, might survive as separate entities to greater heliocentric distances. In that case, the interaction of shocks from adjacent streams may occur while substantial velocity gradients still exist and the details of the subsequent evolution may therefore change somewhat (e.g., see the 1-D calculation by Dryer and Steinolfson, 1976). Moreover Burlaga (1983) suggests that by 25 AU so much interaction of pressure waves will have occurred that deterministic models of the sort used to produce the above plots may not be applicable at all, that a description based upon the concepts of MHD turbulence might be more appropriate. Further justification for such an approach could be taken from considerations of the effects of swept-up transients. It is to be stressed (Burlaga, this Conference; Burlaga *et al.*, 1983) that, at least in the active phase of the solar cycle, embedded transients will severely complicate the structure of the distant solar wind, perhaps to the point of obviating direct modeling efforts.

Be that as it may, the third and final comment I will make on these matters is that it is high time to dispense with these idle speculations and to engage in some serious comparisons between observation and theory. While it is worthwhile and even imperative to attempt conventional radial-alignment mappings with the data in hand, our enthusiasm and expectations must be tempered by the cold realization that most of these observations refer to that period of the solar cycle when the corona is least steady and structured and transient effects are most pronounced. This situation should improve dramatically in the next few years as the sun settles down once again toward solar minimum. For the present, however, far brighter prospects might be in store for a more statistical approach. Obvious tests would include, for example, the radial behavior of the pressure and velocity jumps at shocks, the rate of forward and reverse shock occurrence and decay, the distance to which stream interfaces are visible, the longitudinal structure of the thermodynamic quantities, etc. It may even be possible to pick out newly-formed secondary CIR's as described above and to see if the heliocentric distance of formation agrees with the model predictions. With sufficiently high sampling rates, these structures (if they exist) should stand out by virtue of the close spacing between the forward and reverse shocks and the concomitant high values of density, temperature and field strength, all of which together would be hard to explain in terms of a discrete disturbance propagating all the way from the sun. An important quantitative distinction between the Hundhausen (1973b) hypothesis and MHD models is also amenable to observation. In the hydrodynamic description, CIR shocks in the distant solar wind can actually increase with strength owing to the monotonic decline in sound speed. With the field included, however, the characteristic speed approaches a constant and hence the shock fronts erode more rapidly, thereby providing a measurable discriminant.

Another lucrative endeavor would be to examine rotation-by-rotation averages of interesting quantities like the proton temperature. Earlier theoretical work by Goldstein and Jokipii (1977) suggested significant heating by shock dissipation beyond 2 AU, perhaps resulting in a high-temperature plateau near 5 AU. Heating of the solar wind by interaction with interstellar neutrals might have similar ramifications (Holzer, 1972). Analyses of Pioneer (Mihalov and Wolfe, 1978; Kayser *et al.*, 1983) and Voyager (Gazis and Lazarus, 1982) data, while sorely afflicted with temporal effects, seem to imply a more-

or-less monotonic fall-off in proton temperature of about $r^{-0.5}$ to $r^{-0.7}$. The corresponding predictions of the particular calculation described above (Figure 8) are consistent with these last-quoted values, but it would be desirable to run simulations on other stream data before claiming success. Accurate determination of the average temperature profile may also make it possible to distinguish shock heating from interstellar heating. For example, Figure 8 shows a distinct rapid decline in the mean temperature beyond 20 AU. What is happening in the model is that the velocity jumps are falling below the fast-mode speed (essentially the Alfven speed at these distances), i.e., most of the sawtooths have decayed from shocks into large amplitude MHD waves, which do not contribute to the overall heating. To the contrary, no drop in mean temperature beyond 20 AU would be anticipated if interstellar heating were important. Also, a general rise in the sound speed associated with interstellar heating would tend to erode the saw-tooth velocity features more rapidly than would the simple dynamical process. Hence mere observation of saw-tooths at these distances would lend credence to the dynamic view.

The Effect of Weak Time-Dependence
Upon Stream Evolution

As alluded to above, significant discrepancies between theory and observation persist even when all the dynamic factors included in equations (1) -(4) are accounted for. The worst of these, uncovered by Helios, is illustrated in Figure 9. Each of the panels displays the velocity data from one complete Carrington rotation observed during the Helios A primary mission (Rosenbauer et al., 1977). The data in the top panel were taken when the spacecraft was near 0.98 AU, the next from 0.90 AU, then 0.67 AU, and finally 0.4 - 0.3 AU. The most striking feature is the abrupt, square-wave shape of the perihelion stream (denoted by the arrowhead over the bottom panel). On the basis of early models, such structures (and more were subsequently observed) should give rise to shock pairs well inside 1 AU; but corotating shocks are a very rare phenomenon inside the orbit of earth. More disturbing was the rounding of the stream fronts with radius, which seemed to be totally at odds with established views on stream steepening. With the inclusion of the full list of dynamical mechanisms in (1) -(4), the disagreement was reduced, but not eliminated. Various mechanisms aimed at broadening the streamfronts have since been suggested (e.g. D'Angelo et al., 1979), but these can hardly be regarded as convincing.

I would therefore like to speculate on a possible mechanism that has heretofore been overlooked but is very straightforward and within the grasp of modern computational techniques. Namely, I propose that many of the residual discrepancies between observation and theory can be explained in terms of weak time dependence of the flows emanating from the corona. What I am talking about here is not the impulsive, dramatic outbursts associated with flares and coronal transients, but rather slower, modest temporal effects associated with the ongoing, continual evolution of the corona.

There is solid observational support for change in the corona on all time scales, and I need not belabor the point (e.g. see House, this Conference). Similarly, evidence for interplanetary variability on time scales of the order of a day or two is abundant (Gosling, 1971; Gold et al., this Conference). Explicit insight is to be gained from Figure 10, which shows 1 AU spacecraft observations from J. King's WDC compilation. Depicted are several rotations' worth of velocity data from the most stable period of the solar cycle. While the same pair of streams indisputably recur over and over, detailed differences from rotation to rotation are evident. Substructure with amplitudes of 100-200 km/s comes and goes, and the shape and location of the stream fronts shift back and forth. But how far from the absolutely steady idealization of the models may these temporal variations stray before noticeable effects ensue? And what is the nature of these effects?
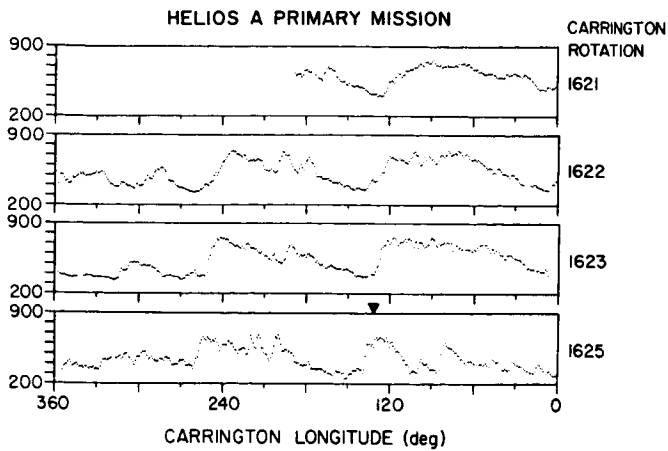
Figure 9). Helios speed data from four Carrington rotations. Perihelion is marked in the bottom panel by the short dark arrow.
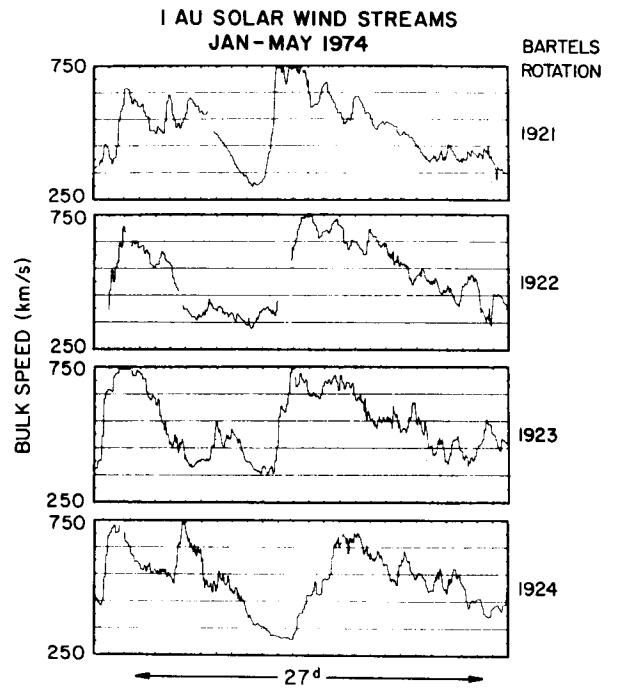

Figure 10). WDC-A 1.0 AU solar wind speed data from four Bartels rotations in 1974.

My ideas on the subject are illustrated in Figure 11. (The visual interpretation of this entire Figure is not immediately obvious, and some reflection may be required to grasp its meaning.) At the top we have a schematic representation of an ideal steady flow, again looking down upon the ecliptic plane from the north. At the $r_0 = 0.2$ AU inner boundary, this simplified solar wind consists of three 90° "sectors" in each of which the flow speed is either uniformly "slow" (light shaded, v = 300 km/s) or uniformly "fast" (medium shaded, v = 500 km/s). All the fluid passing through r_0 in a twelve-hour period is delineated by an arc-shaped "segment". The segments associated with the high-speed flow therefore have 5/3 the radial extent of the slow-flow ones. All the way between r_0 and the $r = 2.0$ AU outer boundary, the evolution is taken to be purely kinematic. The dark-shaded area indicates where the high speed segments overlap the slow-speed segments, corresponding to the compression region in a dynamic model. The white area in the lower left quandrant, where the fast flow has outrun the succeeding slow flow, similarly corresponds to a rarefaction region. Thus Figure 11 is a snapshot of the location of all the fluid segments at some particular instant of time. In this absolutely steady idealization, the boundaries of the various regions are smooth and regular, the flow within each region is totally devoid of substructure, and the entire spiral pattern corotates without real temporal change.

- -

Figure 11), next page. Schematic of (a) strictly-corotating (time-independent) and (b) quasi-steady (weakly time-dependent) solar wind flow. Light shading denotes slow (300 km/s) wind, medium shading denotes high-speed flow (~500 km/s), and dark shading denotes regions where fast and slow flows interact (overlap, in this kinematic projection).

(a)

COROTATING

(b)

WEAKLY
TIME-DEPENDENT
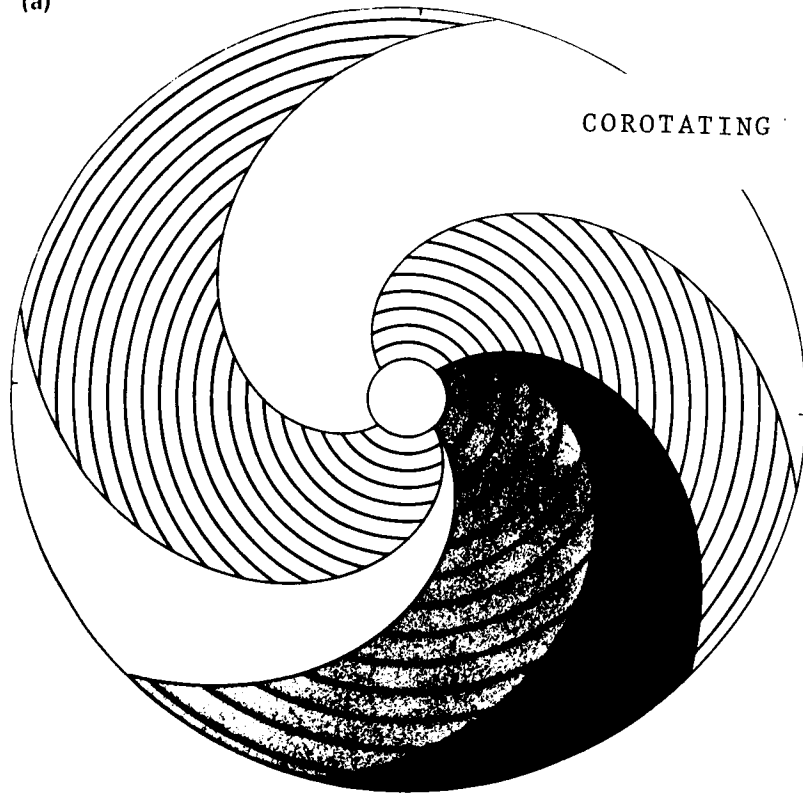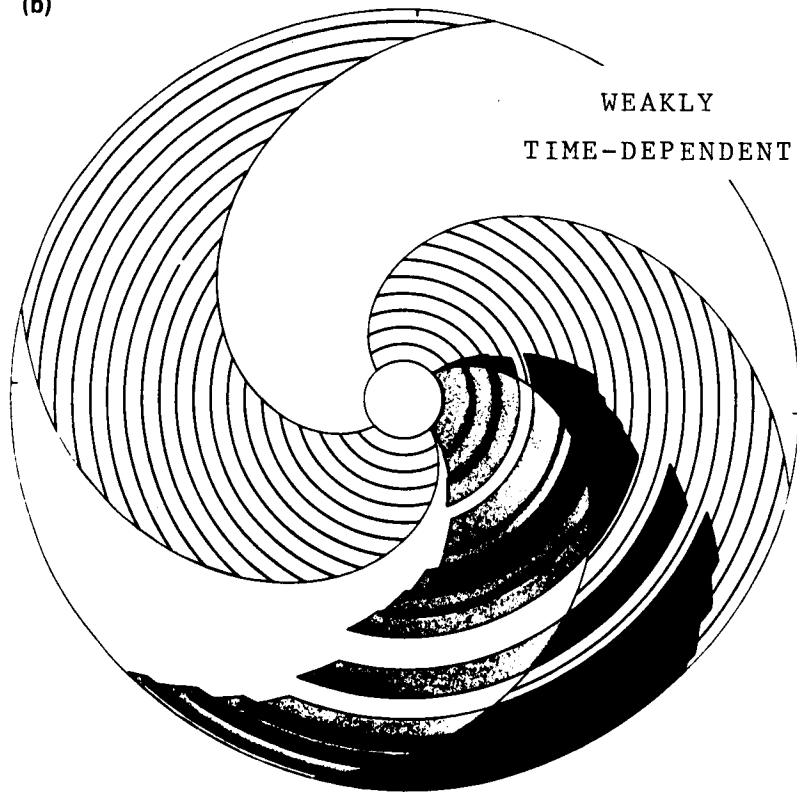
In the lower portion of Figure 11, we consider what happens when a crude time-dependence is introduced. The two slow-flow sectors are kept at 300 km/s as before, but the speed of each segment within the high-speed sector is arbitrarily allowed to change (discontinuously) at the end of every 12-hour interval by a pseudo-random amount within a ± 75 km/s range about 500 km/s. Thus the high speed segments not only overlap the ambient as in the top panel (a), but they also interact with each other. There are two main effects: (1) the boundaries of the "compression" and "rarefaction" regions are no longer smooth and regular, but fluctuate in time and space about the nominal 500 km/s boundaries; and (2), considerable substructure (miniature compressions and rarefactions) has appeared within the high-speed sector. If one now mentally generalizes the picture to allow for variations in the slow flow and furthermore permits longitudinal (and latitudinal) changes as well, it should be evident that though the basic slow-fast-slow structure remains discernible, temporal variations of even this modest amplitude envisioned above should have complicated and perceptible interplanetary consequences.

Qualitatively, we can readily deduce what the most likely observable effects will be. Beyond the trivial conclusions that at least some of the substructure within streams is of temporal origin and that multi-spacecraft and synoptic analyses are impaired by such activity, there should be some important systematic consequences that may not be so obvious. Consider the nature of the substructure engendered by weak time-dependence: it not only has a temporal scale, but a spatial one as well. And from the standpoint of dynamics, it is the spatial scale that is the more significant one. Why so? It has been known for some time that the solar wind acts like a low-pass filter in that small scale variations evolve more rapidly than large scale ones (e.g. Gosling et al., 1976; Hundhausen and Pizzo, unpublished manuscript). Some of this behavior can be seen in the first several panels of Figure 6a, where numerous small scale velocity features at 1 AU have been wiped out by dynamic interaction with adjacent portions of the flow by 4 AU. What this portends for our weakly time-dependent flow is as follows: at any given point, the flow that is observed is the dynamic product of all the fluid "segments" that can reach that point at a given time. Near the sun, say at 0.3 AU, there is not much time for flow segments of differing speeds and times of origin to interact; thus the flow observed, particularly over any suitable short time span such as that required to record the passage of a stream front, is pretty much the instantaneous interplanetary image of the coronal source flow at that time. Farther out, say at 1 AU, many of the segments have had a chance to interact and the resultant flow is no longer a pure image of the coronal flow at any given time; rather it is a mishmash of various flow states, in which a succession of initially-sharp coronal flow boundaries have been transformed into a rounded interplanetary streamfront by the dynamic interaction of the temporally-driven substructure. Finally, at very great heliocentric distances, only the largest spatial scales survive and the evolution proceeds very nearly along the lines of the steady idealization. But even here, the flow seen at, say, 4 AU is not simply related to the coronal source flow at any one particular instant of time; instead, it is more faithfully the image of the composite, dynamically-mixed structure at 1 or 2 AU.

This description has necessarily been qualitative and has resorted to kinematics to press a point. Clearly, quantitative evaluation of these conjectures can only be achieved through the auspices of a full-blown 2-D MHD model, several of which have appeared in the literature (e.g. Nakagawa and Wellck, 1973; D'Uston et al., 1981). Since the precise nature of weak temporal change in the corona is unknown, one of the primary objectives of such a modeling study would be to establish the minimum variation necessary to produce appreciable interplanetary effects. For example, it might be found that minor speed variations along the high-speed low-speed boundary alone could suffice to explain the apparent desteepening of streams. Though such a study would be computationally expensive, I feel confident the results would adequately compensate the efforts and constitute a meaningful contribution to our knowledge of corotating stream dynamics.

Acknowledgements

Bibliography

Burlaga, L. F., Corotating pressure waves with streams in the solar wind, submitted to J. Geophys. Res., 1983.

Burlaga, L. F., and E. Barouch, Interplanetary stream magnetism: Kinematic effects, Astrophys. J. 203, 257, 1976.

Burlaga, L. F., R. Schwenn, and H. Rosenbauer, Dynamical evolution of interplanetary magnetic fields and flows between 0.3 AU and 8.5 AU: Entrainment submitted to Geophys. Res. Lett., 1983.

Carovillano, R. L., and G. L. Siscoe, Corotating structure in the solar wind, Solar Phys. 8, 401, 1969.

D'Angelo, N. D., G. Joyce, and M. E. Pesses, Landau damping effects on solar wind fast streams, Astrophys. J. 229, 1138, 1979.

Dryer, M., Z. K. Smith, E. J. Smith, J. D. Mihalov, J. H. Wolfe, R. S. Steinolfson, and S. T. Wu, Dynamic MHD modeling of solar wind corotating stream interaction regions observed by Pioneer 10 and 11, J. Geophys. Res. 83, 4347, 1978.

Dryer, M., and R. S. Steinolfson, MHD solution of interplanetary disturbances generated by simulated velocity perturbations, J. Geophys. Res. 81, 5413, 1976.

D'Uston, C., M. Dryer, S. M. Han, and S. T. Wu, Spatial structure of flare-associated perturbations in the solar wind simulated by a two-dimensional numerical MHD model, J. Geophys. Res. 86, 525, 1981.

Gazis, P. R., and A. J. Lazarus, Voyager observations of solar wind proton temperature: 1 - 10AU, Geophys. Res. Lett. 9, 431, 1982.

Goldstein, B. E., Nonlinear corotating solar wind structure, Rep. CSR-P-71-63, Mass. Inst. of Technol., Cambridge, 1971.

Goldstein, B. E., and J. R. Jokipii, Effects of stream-associated fluctuations upon the radial evolution of average solar wind parameters, J. Geophys. Res. 82, 1095, 1977.

Gosling, J. T., Variation in the solar wind speed along the Earth's orbit, Solar Phys. 17, 499, 1971.

Gosling, J. T., A. J. Hundhausen, V. Pizzo, and J. R. Asbridge, Compressions and Rarefactions in the solar wind: Vela 3, J. Geophys. Res. 77, 5442, 1972.

Gosling, J. T., A. J. Hundhausen, and S. J. Bame, Solar wind stream evolution at large heliocentric distances: Experimental demonstration and the test of a model, J. Geophys. Res. 81, 2111, 1976.

Gosling, J. T., J. R. Asbridge, S. J. Bame, and W. C. Feldman, Solar wind stream interfaces, J. Geophys. Res. 83, 1401, 1978.

Holzer, T. E., Interaction of the solar wind with the neutral component of the interstellar gas, J. Geophys. Res. 77, 5407, 1972.

Hundhausen, A. J., Nonlinear model of high-speed solar wind streams, J. Geophys. Res. 78, 1528, 1973a.

690

Hundhausen, A. J., Evolution of large-scale solar wind structures beyond 1 AU, J. Geophys. Res., 78, 2035, 1973b.

Hundhausen, A. J., and J. T. Gosling, Solar wind structure at large solar heliocentric distances: An interpretation of Pioneer 10 observations, J. Geophys. Res., 81, 1436, 1976.

Hundhausen, A. J., and L. F. Burlaga, A model for the origin of solar wind stream interfaces, J. Geophys. Res., 80, 1845, 1975.

Jokipii, J. R., and L. Davis, Jr., Long-wavelength turbulence and the heating of the solar wind, Astrophys. J., 156, 1101, 1969.

Kayser, S. E., A. Barnes, and J. D. Mihalov, The far reaches of the solar wind: Pioneer 10 and 11 plasma results, submitted to Astrophys. J.

Matsuda, T., and T. Sakurai, Dynamics of the azimuthally-dependent solar wind, Cosmic Electrodynamics, 3, 97, 1972.

Mihalov, J. D., and J. H. Wolfe, Pioneer-10 observation of the solar wind proton temperature heliocentric gradient, Solar Phys., 60, 399, 1978.

Nolte, J. T., A. S. Krieger, E. C. Roelof, R. E. Gold, High coronal structure of high velocity solar wind stream sources, Solar Phys., 51, 459, 1977.

Nakagawa, Y., and R. E. Wellck, Numerical studies of azimuthal modulation of the solar wind with magnetid fields, Solar Phys., 32, 257, 1973.

Pizzo, V., A three-dimensional model of corotating streams in the solar wind. 1. Theoretical Foundations, J. Geophys. Res., 83, 5563, 1978.

Pizzo, V., An evaluation of corotating stream models, in Solar Wind Four, MPAE-W-100-81-31, H. Rosenbauer, ed., p. 153, 1981.

Pizzo, V., A three-dimensional model of corotating streams in the solar wind. 3. Magnetohydrodynamic streams, J. Geophys. Res., 87, 4374, 1982.

Riesebieter, W., Dreidimensionale Modelrechnungen zum solaren Wind, Ph. D. thesis, Tech. Univ. zu Braunschweig, Federal Republic of Germany, 1977.

Rosenbauer, H., R. Schwenn, E. Marsch, B Meyer, H. Miggenrieder, M. D. Montgomery, K. H. Muhlhauser, W. Pilipp, W. Voges, and S. M. Zink, A survey of initial results of the Helios plasma experiment, J. Geophys., 42, 561, 1977.

Siscoe, G. L., Structure and orientation of solar wind interaction fronts: Pioneer 6, J. Geophys. Res., 77, 27, 1972.

Sittler, E. C. Jr., and J. D. Scudder, An empirical polytrope law for solar wind thermal electrons between 0.45 and 4.67AU: Voyager 2 and Mariner 10, J. Geophys. Res., 85, 5131, 1980.

Smith, E. J., and J. H. Wolfe, Observations of interaction regions and corotating shocks between one and five AU: Pioneers 10 and 11, Geophys. Res. Lett., 3, 137, 1976.

Steinolfson, R. S., M. Dryer, and Y. Nakagawa, Numerical MHD simulation of interplanetary shock pairs, J. Geophys. Res., 80, 1223, 1975.

Whang, Y. C., Magnetohydrodynamics of corotating interplanetary structures, J. Geophys. Res., 85, 2285, 1980.

Whang, Y. C., and T. H. Chien, Magnetohydrodynamic interaction of high-speed streams, J. Geophys. Res., 86, 3263, 1981.